

pubs.acs.org/JPCL Letter

# Molecular Control of Floquet Topological Phase in Non-adiabatic Thouless Pumping

Ruiyi Zhou and Yosuke Kanai\*



Cite This: J. Phys. Chem. Lett. 2023, 14, 8205-8212



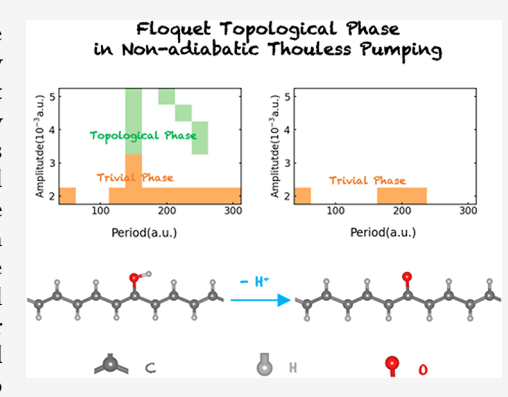
**ACCESS** I

III Metrics & More

Article Recommendations

Supporting Information

**ABSTRACT:** Non-adiabatic Thouless pumping of electrons is studied in the framework of topological Floquet engineering, particularly with a focus on how atomistic changes to chemical moieties control the emergence of the Floquet topological phase. We employ real-time time-dependent density functional theory to investigate the extent to which the topological invariant, the winding number, is impacted by molecular-level changes to *trans*-polyacetylene. In particular, several substitutions to *trans*-polyacetylene are studied to examine different effects on the electronic structure, including the mesomeric effect, inductive effect, and electron conjugation effect. Maximally localized Wannier functions are employed to relate the winding number to the valence bond description by expressing the topological pumping as the transport dynamics of the localized Wannier functions. By further exploiting the gauge invariance of the quantum dynamics in terms of the minimal particle—hole excitations, the topological pumping of electrons can be also



represented as a cyclic transition among the bonding and antibonding orbitals. Having connected the topological invariant to the chemical concepts, we demonstrate molecular-level control of the emergence of the Floquet topological phase, presenting an exciting opportunity for the intuitive engineering of molecular systems with such an exotic topological phase.

ne of the earliest realizations that topological characteristics of the Hamiltonian govern certain dynamical properties came from Thouless when he discussed the quantized pumping phenomenon in 1983. Studying onedimensional quantum-mechanical particle transport in a slowly varying potential, he showed that the quantization of the number of transported quantum particles is derived from the topology of the underlying Hamiltonian. Under adiabatic evolution (i.e., instantaneous eigenstates of the Hamiltonian), the particle current in a one-dimensional system is given by the topological quantity called the winding number when the Hamiltonian is periodic in time. For topological materials, the winding number can take a nonzero integer value, whereas it is zero for normal/trivial insulators. In recent years, Thouless pumping has been demonstrated experimentally in various systems, 2-5 including an ultracold Fermi gas and ultracold atoms in an optical lattice. Various theoretical studies<sup>8–11</sup> have employed model Hamiltonians such as the Rice-Mele model, 12 and the description of topological pumping has often assumed complete adiabaticity of the Hamiltonian evolution. At the same time, studies of non-adiabatic effects on Thouless pumping have appeared in the literature. 13-15 A particularly notable development in recent years has been the idea of socalled topological Floquet engineering, in which one uses a time-periodic field to induce topological properties in a driven system that is otherwise a trivial insulator. <sup>16,17</sup> In a Floquet system, the time-dependent Hamiltonian satisfies  $\hat{H}(t + T) =$ H(t) and the time-independent effective Hamiltonian can be

defined from the time evolution operator. One can analogously apply the topological description to this effective Hamiltonian. Under certain conditions, the Floquet topological phase, in which the winding number is a nonzero integer, can emerge. In our previous work using first-principles theory, 18 we showed that such a topological phase can be present for a transpolyacetylene polymer chain using the external electric field as the driving field for the Floquet condition. We have also shown that the Floquet topological phase can be directly linked to the well-established description of valence bond theory. There is an increasing effort to develop a molecular-level understanding of topological materials from the perspective of chemistry, 19which would open up the field for exploration with a more intuitive viewpoint based on the arrangement of atoms. Having established the connection between the Floquet topological phase in the Thouless pump and the valence bond description, 18 an important question now is to what extent this topological phenomenon can be controlled rationally in terms of chemical understanding.

Received: June 26, 2023 Accepted: August 25, 2023



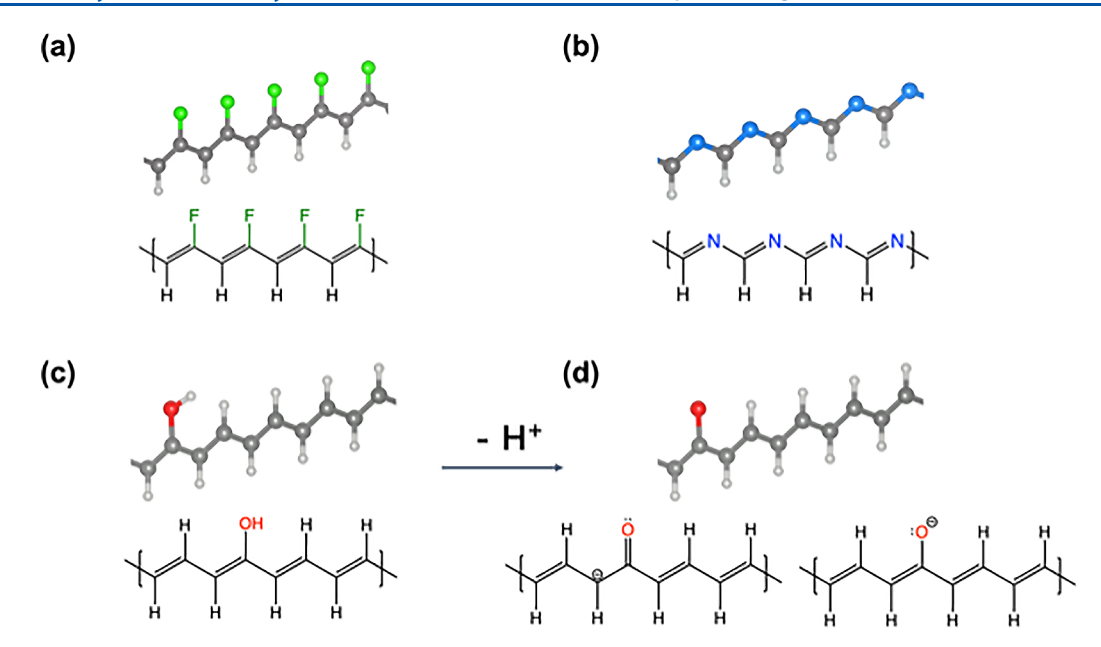


**Figure 1.** Chemical structures of the four substituted *trans*-polyacetylene systems studied in this work. (a) Fluorine substitution of C–H bonds in *trans*-polyacetylene. (b) Nitrogen substitution of C–C bonds in *trans*-polyacetylene. (c) Enol (OH) substitution at a single C–H bond as the "defect" site. (d) Enolate ion (O<sup>-</sup>) substitution at a single C–H bond as the "defect" site.

Let us briefly recap the theoretical formulation presented in our recent work. 18 One can show that the particle current in a one-dimensional (1D) system is given by the topological invariant called the winding number when the Hamiltonian is time-periodic. For the topological phase, the winding number can take a nonzero integer value, whereas it is zero for a normal/trivial insulator. This intricacy of the Hamiltonian can be recovered conveniently from the phase information in quantum-mechanical wave functions (particularly important for studying real systems instead of model Hamiltonians), and it has a close connection to the modern theory of polarization developed in the 1990s.<sup>23</sup> In topological Floquet engineering, a time-periodic field is used to induce a topological phase in the driven system that is otherwise a trivial insulator. 16,17 In a Floquet system, the time-dependent Hamiltonian satisfies  $\hat{H}(t)$ + T) =  $\hat{H}(t)$ , and a time-independent effective Hamiltonian can be defined from the evolution operator over one time period T such that  $\hat{H}_{\rm eff}(k) \equiv i\hat{T}^{-1} \ln \hat{U}(k)$ , where  $\hat{U}(k) \equiv \hat{\mathcal{T}} \exp \left[ -i \int_0^T dt \ \hat{H}(k, t) \right]$ , in which  $\hat{\mathcal{T}}$  is the timeordering operator and *k* is the reciprocal wave vector of the 1D system. Extending to the non-adiabatic regime, the winding number, being equal to the integrated particle current over the periodic time T, can be given in terms of the energy spectrum of the effective Floquet Hamiltonian,  $\varepsilon_i$  (quasi-energy)<sup>24</sup> or equivalently in terms of the non-adiabatic Aharonov-Anandan geometric phases<sup>25</sup> of its eigenstates,  $\Phi_i$ . Conveniently for electronic structure theory, the winding number can be written

$$\begin{split} W &= \frac{1}{2\pi} \int_{-\pi}^{\pi} \mathrm{d}k \sum_{i}^{\mathrm{occ}} \langle \Phi_{i}(k, t=0) | \hat{U}^{\dagger}(k) \mathrm{i} \partial_{k} \hat{U}(k) | \Phi_{i}(k, t=0) \rangle \\ &= \frac{1}{2\pi} \sum_{i}^{\mathrm{occ}} \left[ \int_{BZ} \mathrm{d}k \; \langle u_{i}(k, t=T) | \mathrm{i} \partial_{k} | u_{i}(k, t=T) \rangle \right. \\ &\left. - \int_{BZ} \mathrm{d}k \; \langle u_{i}(k, t=0) | \mathrm{i} \partial_{k} | u_{i}(k, t=0) \rangle \right] \end{split} \tag{1}$$

where  $u_i(k,t)$  are the time-dependent Bloch states. One notes that the winding number is expressed analogously to the static Chern insulator as  $W=C\equiv \frac{1}{2\pi}\int_0^T \mathrm{d}t \int_{BZ} \mathrm{d}k \sum_i^{\mathrm{occ.}} F_i(k,t)$ , where C is the first Chern number and  $F_i(k,t)$  is the generalized Berry curvature, given by  $F_i(k,t)=\mathrm{i}[\langle \partial_i u_i(k,t)|\partial_k u_i(k,t)\rangle - \langle \partial_k u_i(k,t)|\partial_i u_i(k,t)\rangle].^{26}$  Due to the Blount identity,  $\langle w_i(t)|\hat{r}|w_i(t)\rangle = \frac{L}{2\pi}\int_{BZ}\mathrm{d}k \langle u_i(k,t)|\mathrm{i}\partial_k |u_i(k,t)\rangle$ , the winding number can be expressed in terms of the time-dependent maximally localized Wannier functions (MLWFs),  $w_i(r,t)$ , as  $^{18}$ 

$$W = L^{-1} \sum_{i}^{\text{occ.}} \left[ \langle w_i(t=T) | \hat{r} | w_i(t=T) \rangle - \langle w_i(t=0) | \hat{r} | w_i(t=0) \rangle \right]$$
(2)

where the position operator is defined according to the formula given by Resta for extended periodic systems  $^{27}$  and L is the lattice length of the unit cell. The winding number is then equal to the number of geometric centers of the MLWFs (i.e., Wannier centers) transported over one periodic time T.  $^{24,28}$ This provides a real-space description of how the winding number physically represents the number of electrons pumped in the time T. The Kohn-Sham (KS) ansatz of density functional theory (DFT) offers a convenient (and in principle exact) description for utilizing this single-particle theoretical formalism in studying real systems.<sup>29–36</sup> However, an additional mathematical complication exists because the KS Hamiltonian depends on the time-dependent electron density or the underlying KS orbitals. Therefore, the Floquet condition (i.e.,  $\hat{H}_{KS}(t+T) = \hat{H}_{KS}(t)$ ) is not always satisfied for the KS ansatz even when the external driving field is time-periodic in T, and the Floquet condition can be obtained only for some sets of the driving fields. In our previous work, 18 it was numerically shown that the time-integrated particle current Q is indeed an integer as expected, being equal to the winding number W when the Floquet condition is satisfied. We demonstrated non-adiabatic Thouless pumping of electrons by

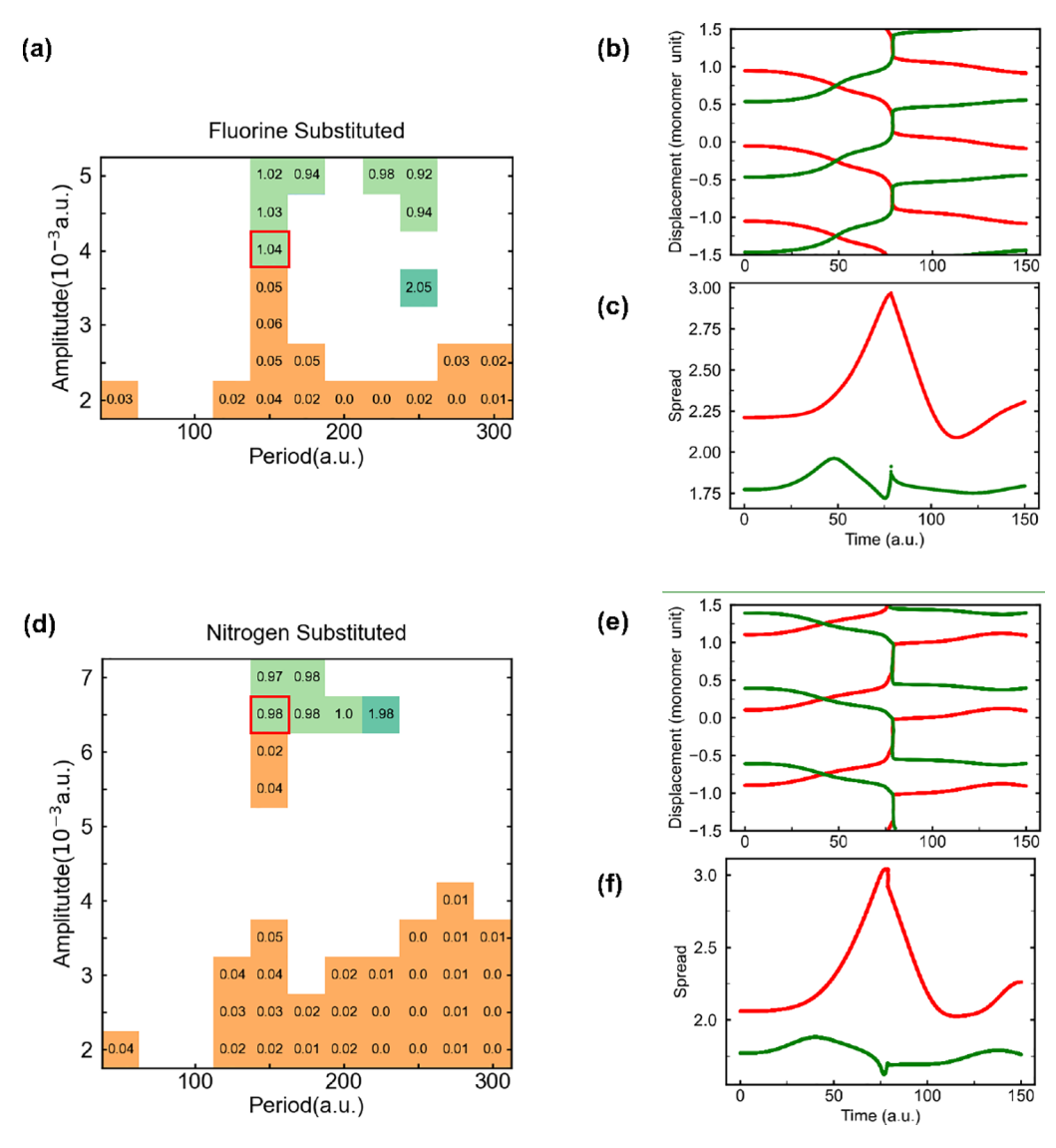


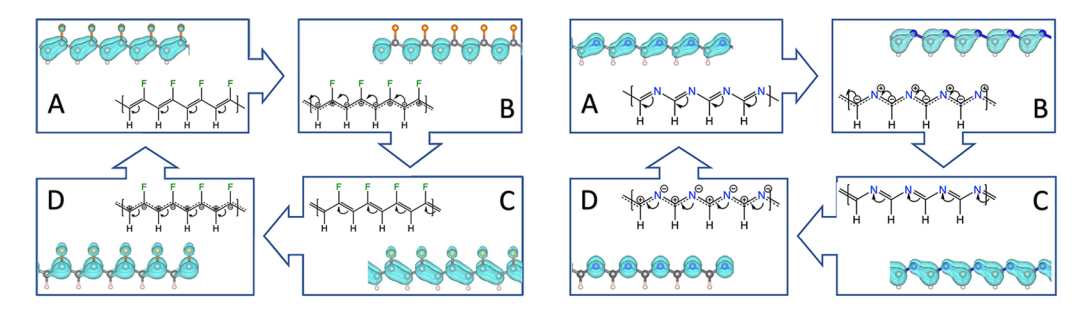
Figure 2. Time-integrated current over one driving cycle,  $Q_i$  for (a) fluorine-substituted and (d) nitrogen-substituted trans-polyacetylene as a function of the electric field amplitude |A| and the time period T. The white (colorless) areas represent that the Floquet condition is not satisfied. The red square indicates the specific Floquet condition (W = 1 topological phase) for which the MLWF dynamics was analyzed in detail. For this specific case, the dynamics of the MLWF is shown: the displacements of MLWF centers with C = C/C = N bonds (red) and C = C/C = N bonds (green) are shown for (b) fluorine substitution and (e) nitrogen substitution, and spread values for MLWFs are shown for (c) fluorine substitution and (f) nitrogen substitution.

locating the Floquet topological phase (i.e.,  $W \neq 0$ ) for *trans*-polyacetylene. A brief discussion of our previous findings for unsubstituted *trans*-polyacetylene can be found in the Supporting Information.

An important question is to what extent the emergence of the Floquet topological phase, where the winding number is a nonzero integer, is susceptible to molecular-level changes and whether it can be controlled rationally using our chemical insights. In order to examine these aspects, in this work we make atomistic changes to *trans*-polyacetylene and study how these changes impact the Floquet topological phase. We consider four related systems, as shown in Figure 1. Fluorine substitution of C–H bonds in *trans*-polyacetylene (Figure 1a) is used to study the mesomeric effect; H atoms are substituted by electron-donating F atoms on one side of the carbon chain. Nitrogen atom substitution of C–C bonds (Figure 1b) is used to study the inductive effect, which results in charge polarization along the backbone. One of the two distinct

carbon atoms in individual monomer units is replaced with a N atom, which has a higher electronegativity. We further consider the polyacetylene system with a single C-H bond substituted at a "defect" site by enol (OH) and enolate ion (O $^-$ ) forms, as shown in Figure 1c,d, respectively. The enolate ion case is particularly interesting because the valence bond model yields a well-recognized resonance structure with a C=O double bond, disrupting the electron conjugation on the carbon chain.

Figure 2a shows the calculated (time-)integrated current, Q, per monomer for the F-substituted case as a function of the driving field amplitude and period. In the figure, the white (colorless) areas indicate those amplitude/period combinations for which the Floquet condition is not met, so that the Floquet engineering cannot be applied for analysis. As can be seen in Figure 2a, Q is quantized as expected when the Floquet condition is satisfied, and it is equal to the winding number (i.e., Q = W) within the numerical accuracy anticipated from the RT-TDDFT simulation. For those cases in which the



### Fluorine Substituted

# Nitrogen Substituted

Figure 3. Selected snapshots of the most dominant dynamical transition orbital (DTO) in one driving cycle for the fluorine substitution and nitrogen substitution cases, with corresponding Lewis structures illustrating the electronic structure changes for the W = 1 Floquet topological phase with T = 150 au/|A| = 0.00400 au (fluorine substitution) and T = 150 au/|A| = 0.00650 au (nitrogen substitution).

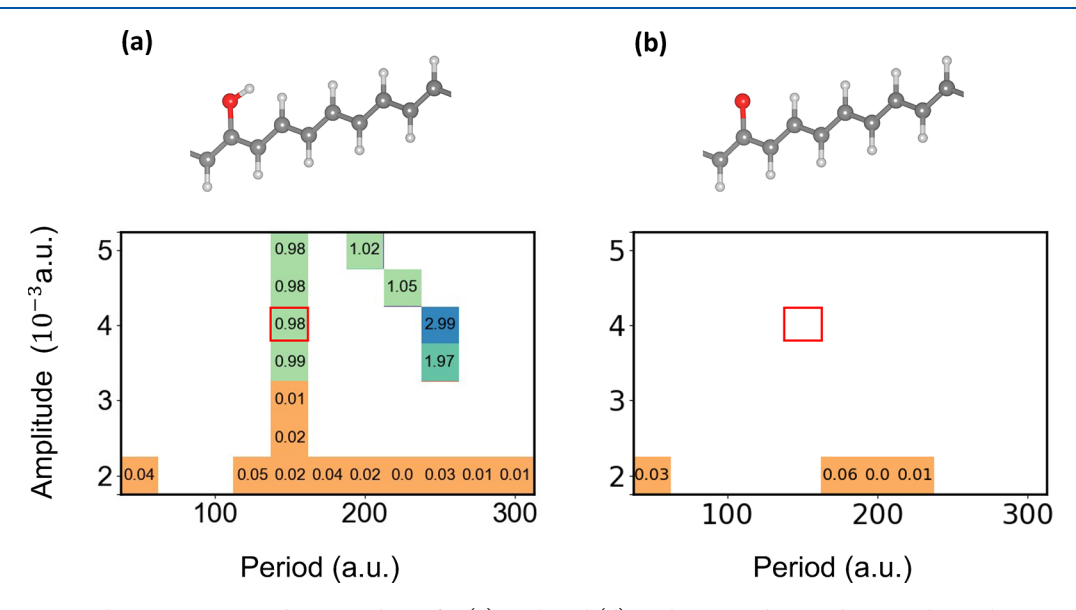


Figure 4. Time-integrated current over one driving cycle, Q, for (a) enol- and (d) enolate ion-substituted *trans*-polyacetylene as a function of the electric field amplitude |A| and the time period T. The white (colorless) areas represent that the Floquet condition is not satisfied. The red square indicates the specific driving field for which the MLWF dynamics was analyzed in detail.

driving field amplitude is small, the winding number is zero, and normal/trivial phase is present. For other areas, the topological phase can be identified, such that the winding number is a nonzero integer. Although the exact combinations of the field amplitude and period for observing the Floquet topological phase differ from those of unsubstituted transpolyacetylene (Figure S1), the qualitative features are the same. This is perhaps expected since the F substitution does not significantly disrupt the electron conjugation, which was found to be important for the topological pumping. 18 At the same time, the dynamics of the MLWFs show discernible differences. Let us focus on the specific case of the driving field with T = 150 au and |A| = 0.0040 au (W = 1) for detailed discussion. Figure 2b shows that Wannier centers are transported much more abruptly when C-C and C=C Wannier centers cross among them (at  $t \sim 1/2T$ ) as in the quantum-tunneling-like behavior observed in ref 37, and their MLWF spreads become somewhat larger to the values of 1.92 and 2.96 au<sup>2</sup> for C-C and C=C MLWFs, respectively (see Figure 2c).

The dynamical transition orbital (DTO) gauge<sup>38</sup> provides a convenient description of the topological pumping in terms of

minimal particle—hole excitations as discussed in ref 18. In particular, the single DTO orbital,  $\varphi_1^{\rm DTO}({\bf r},t)$ , was found to be largely responsible for the topological pumping. Figure 3 shows how this particular DTO orbital transforms from having  $\pi$  bonding orbital character at equilibrium to acquiring resonance and  $\pi^*$  antibonding character in a single driving cycle. Overall, the DTO transformation for the F-substituted system is similar to that of the unsubstituted case, but with one notable difference. Due to the mesomeric effect, the lone-pair electrons on F atoms shift the  $\pi$  electron density distribution, resulting in a noticeable delocalization of the DTO orbital over to the F atoms. However, the F substitution does not severely disrupt the electron conjugation, which is important for topological pumping, and the DTO transformation remains largely the same as for the unsubstituted case.

Figure 2d shows the integrated current, *Q*, for the nitrogensubstituted case. Just as in the case of the F substitution of H atoms, the N substitution of C atoms in polyacetylene retains the existence of the Floquet topological phase. The valence bond model argument would suggest that the electron conjugation is preserved along the C/N chain, and the MLWFs indeed show the alternating arrangement for the double/single C-N bonds (Figure 2e). At the same time, the C-N bonds are significantly polarized due to the high electronegativity of the nitrogen atoms. As can be seen in Figure 2d, the Floquet topological phase is still observed in this case, but with driving fields that are quite different from those for the unsubstituted trans-polyacetylene case. In particular, a higher field amplitude (a minimum of |A| = 0.0065 au) was necessary to induce the W = 1 Floquet topological phase. This is likely due to the highly polarized nature of the C-N chain. Nitrogen atoms are more electronegative than carbon atoms, and a stronger perturbation is likely needed for the pumping of electrons than for the unsubstituted C-C chain case. Indeed, the DTO shows noticeably enhanced localization on nitrogen atoms compared with carbon atoms, as shown in Figure 3 at t = 0 au with no driving field. Focusing on the specific condition of the driving field with  $T = 150 \text{ au/}|\mathbf{A}| = 0.0065 \text{ au}$  (W = 1), the Wannier center dynamics shows features that are very much like the F substitution case as shown in Figure 2e. The tunneling-like behavior was again observed here, and the MLWF spreads for the C-N and C=N bonds become somewhat larger to the values of 1.67 and 3.04 au<sup>2</sup>, respectively (see Figure 2f).

The tautomerism between  $-\mathrm{O}^-$  and  $-\mathrm{OH}$  substitutions at a C-H bond (Figure 1) represents a particularly interesting example for examining the relationship between electron conjugation and Thouless topological pumping. Structurally, these two cases are quite similar and related only by a difference of a single proton. Figure 4 shows the integrated current, Q, for these two cases. Even though these two structures are closely related by a single proton, only the enol ( $-\mathrm{OH}$ ) case yields the Floquet topological phase where the winding number, W, is a nonzero integer, while the enolate ( $-\mathrm{O}^-$ ) case yields only the trivial insulator phase (i.e., W=0).

Even though these two cases are structurally quite similar, their valence bond structures are quite distinct. When a single enolate ion  $(-O^{-})$  is present, multiple resonance structures can be drawn by invoking simple valence bond theory considerations, as shown in Figure 1d. In particular, one might easily depict a C=O double bond. Such a valence bond structure would result in the formation of a domain wall, disrupting the electron conjugation along the carbon chain. In order to relate the existence/absence of the Floquet topological phase to a simple valence bond description, let us first discuss the MLWFs in the equilibrium state with no driving field applied. The enolate ion  $(-O^{-})$  structure contains three lone-pair MLWFs associated with the oxygen atom, while the enol (-OH) structure contains two oxygen lone-pair MLWFs and one O-H bond MLWF. Table 1 shows that the MLWF spread of the C-O bond does not change significantly (only by  $\sim 0.02$  au<sup>2</sup>) when the proton is removed from the enol

Table 1. Spread Values (in au<sup>2</sup>) of the MLWFs in the Enol (-OH)- and Enolate Ion (-O<sup>-</sup>)-Substituted Cases; Values in Parentheses Are the Standard Deviations among the MLWFs for Each Bond Type

MLWF	ОН	O <sup>-</sup>
lone pair	1.4829/1.4829	2.3021/2.3019
O-H bond/lone pair	1.6133	1.7499
C-O bond	1.3409	1.3637
C=C	2.3048 (0.0328)	2.4098 (0.2358)
C-C	1.7701 (0.0067)	1.7928 (0.0381)

(-OH) structure. However, the other three MLWFs localized on the oxygen atom become highly delocalized. Individual MLWFs in the enolate ion structure have a shape similar to that of those in the enol form (see Figure S6). However, when compared with the enol form, the three lone-pair MLWFs in the enolate ion are spatially more delocalized (i.e., the spread values increase by approximately 0.83 au<sup>2</sup>) with a significant contribution from adjacent carbon atoms. They indicate that parts of the lone-pair electrons on the oxygen atom for the enolate ion (-O<sup>-</sup>) are indeed involved in the conjugated carbon bonds through resonance, as depicted in the resonance structures (Figure 1d). At the same time, the C-C/C=CMLWFs in the enol (-OH) form are the same as in the unsubstituted trans-polyacetylene case, with essentially the same MLWF spread values. The spread values of these C-C/ C=C MLWFs do not vary among the monomer units, irrespective of their locations from the -OH defect site. However, in the enolate ion  $(-O^{-})$  form, the spread values of these MLWFs vary significantly along the C-C chain depending on their location from the  $-O^-$  defect site.

Let us now examine the Wannier center dynamics to gain further insights into how the Floquet topological phase emerges in the enol (-OH) form while it is absent in the enolate ion  $(-O^{-})$  form despite their seemingly minor difference. As a representative case, we examine the specific condition of the driving field with  $T = 150 \text{ au/}|\mathbf{A}| = 0.00400$ ; the W = 1 Floquet topological phase is found for the enol form, while the Floquet condition is not satisfied for the enolate ion form. Figure 5 shows that the quantum transport characteristics are completely changed by the removal of a single proton. For the enol (-OH) structure, the dynamics of MLWFs is essentially identical to that of unsubstituted trans-polyacetylene, and the MLWF spreads do not vary much among the MLWFs and also do not change much in time (Figure 5a). However, for the enolate ion  $(-O^{-})$  form, the MLWF spreads vary considerably over time, depending on their locations with respect to the  $-O^-$  defect site (Figure 5b). The Wannier center dynamics for the enol and enolate forms are initially quite similar, such that they move in the same direction continuously (Figure 5c,d). However, for the enolate ion (-O<sup>-</sup>) form, C=C and C-C Wannier centers begin to reverse their movement in the opposite direction at t = 100— 150 au. The rates at which the C=C and C-C Wannier centers change their directions depend on their distances from the -O defect site, and the -O defect effectively forms a domain wall such that MLWFs are prevented from being transported to the C atom on the opposite side across this defect site.

The quantum dynamics of electrons still can be largely modeled from the dynamics of a single DTO orbital for both the enolate ion and enol structures. For the enol (-OH) case, the particle population of this DTO orbital decays back to zero, as shown in Figure 6a, as perhaps expected from having the Floquet condition satisfied. For the enolate ion form, the population does not decay back to zero, while this particular DTO is still largely reponsible for the whole quantum dynamics of electrons, as seen in Figure 6b. Snapshots of the DTO orbital transformation for both structures are also shown in Figure 6. For the enol structure, the introduction of the -OH substituent group has little effect on the topological pump, as can be seen in Figure 6a. The DTO transformation shows the changes from having  $\pi$  bonding orbital character at equilibrium to acquiring resonance and  $\pi^*$  antibonding

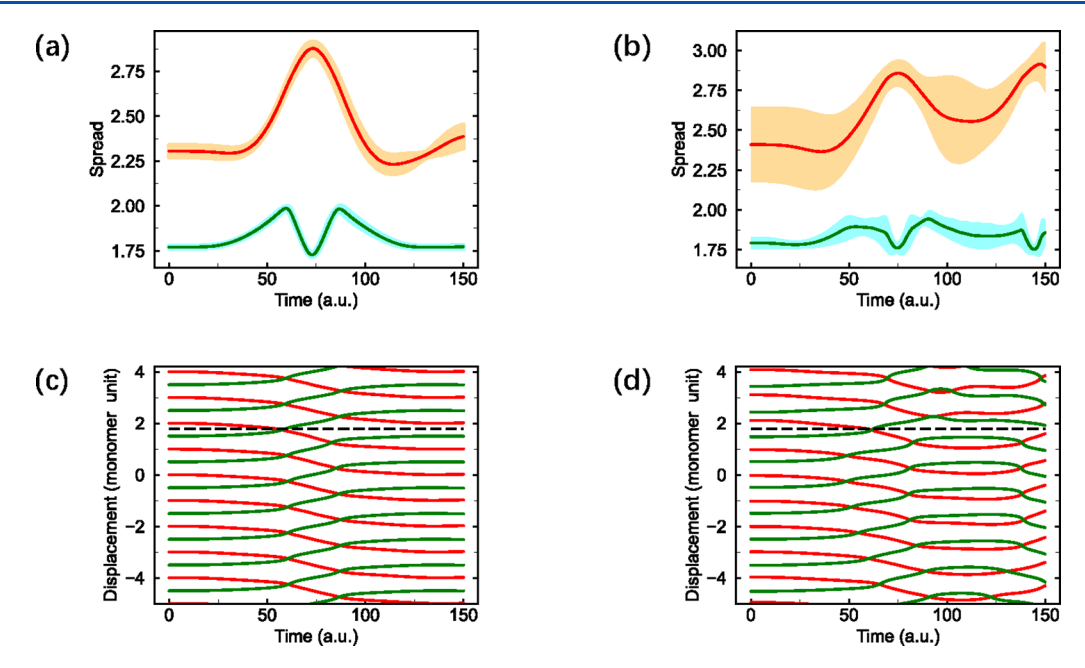
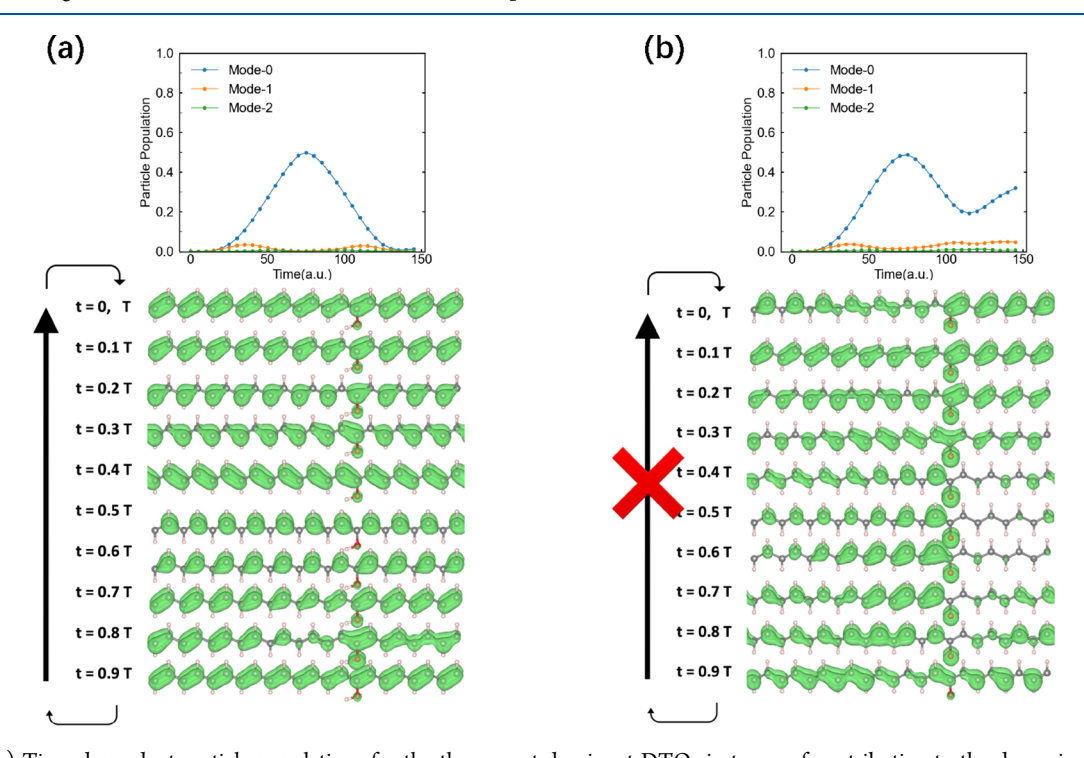


Figure 5. MLWF dynamics for the enol (-OH) and enolate ion  $(-O^-)$  substitutions in *trans*-polyacetylene with the driving field of T = 150 au/lAl = 0.00400 au. (a, b) Spread values for (a) enol and (b) enolate ion substitution. The average values are shown by the solid lines for C = C (red) and C = C (green) MLWFs, while the shaded regions indicate the standard deviations among the MLWFs for each bond type. (c, d) Displacement of MLWF centers for (c) enol and (d) enolate ion substitution. The red and green solid lines show the displacements of individual centers for C = C (red) and C = C (green) MLWFs, and the dashed lines mark the positions of the C = C (red) and C = C (green) MLWFs, and the dashed lines mark the positions of the C = C (red) and C = C (green) MLWFs, and the dashed lines mark the positions of the C = C (red) and C = C (green) MLWFs, and the dashed lines mark the positions of the C = C (red) and C = C (green) MLWFs, and the dashed lines mark the positions of the C = C (red) and C = C (green) MLWFs, and the dashed lines mark the positions of the C = C (red) and C = C (green) MLWFs, and the dashed lines mark the positions of the C = C (red) and C = C (green) MLWFs, and the dashed lines mark the positions of the C = C (red) and C = C (green) MLWFs, and the dashed lines mark the positions of the C = C (red) and C =



**Figure 6.** (top) Time-dependent particle populations for the three most dominant DTOs in terms of contributing to the dynamics and (bottom) snapshots of the most dominant DTO in a single driving cycle with the driving field of T = 150 au/|A| = 0.00400 au for the (a) enol (-OH) and (b) enolate ion (-O<sup>-</sup>) substitutions.

character in a single driving cycle, exactly like for the unsubstituted case. However, Figure 6b shows that the DTO transformation is quite different in the case of the enolate ion  $(-O^-)$  structure, for which the Floquet topological phase is absent. Even at t=0 with no driving field, the DTO appears substantially different from the unsubstituted case (see Figure S2). The observed DTO transformation (Figure 6b) is such

that it is not possible to interpret its changes simply as the particle—hole transition between the  $\pi$  and  $\pi^*$  orbitals. Indeed, for the enolate ion  $(-O^-)$  case, the DTO orbital does not return to its original form at the end of the driving cycle, as the Floquet condition is not satisfied.

Non-adiabatic Thouless pumping of electrons was studied with first-principles theory in the framework of topological

Floquet engineering, specifically focused on how molecular changes to chemical moieties of trans-polyacetylene impact the emergence of the Floquet topological phase. In particular, we considered several molecular-level substitutions to examine different types of effects on the electronic structure, including the mesomeric effect, the inductive effect, and the electron conjugation effect, based on our earlier analysis of the topological phase using the valence bond model. 18 For the cases of the substitution of hydrogen atoms with fluorine atoms (the mesomeric effect) and the substitution of carbon atoms with nitrogen atoms (the inductive effect), the Floquet topological phase is still present, even though the specific driving field necessary for inducing the topological phase is changed. We also considered the case in which a H atom on a C-H bond was substituted with either a OH or O<sup>-</sup> group. Interestingly, the seemingly innocuous change of C-OH to its enolate ion (C-O<sup>-</sup>) form, related by a single proton, leads to the disappearance of the Floquet topological phase. This finding was rationalized by invoking the valence bond theory description, as the enolate ion form yields a prominent resonance structure with C=O bond characteristic. The Floquet topological phase disappears because the electronic conjugation along the carbon chain is disrupted by the C=O resonance structure. In summary, by connecting the topological invariant (i.e., the winding number) to the chemically intuitive picture of valence bond theory, we have discussed how molecular changes to trans-polyacetylene impact its Floquet topological phase. The molecular-level understanding from our first-principles simulation yielded an important step toward the systematic and intuitive design of chemical systems for the emergence of such an exotic topological phase. As in most theoretical works on topological materials, the atomic dynamics on the electronic Hamiltonian were not studied in this work. Our future work will examine the influence of the electronic current on the atomic lattice dynamics and reciprocally their impact on the non-adiabatic Thouless pumping of electrons as well as thermal effects on the atomic lattice.

# COMPUTATIONAL METHODS

Real-time time-dependent density functional theory (RT-TDDFT)<sup>39,40</sup> simulations were performed using the Qb@ll branch<sup>31,41–43</sup> of the Qbox code<sup>44</sup> within the plane-wave pseudopotential (PW-PP) formalism.<sup>45</sup> A 55-atom simulation supercell, consisting of 11 C-C monomer units aligned along the x axis, was employed along with the periodic boundary conditions (51.32 bohr  $\times$  15.0 bohr  $\times$  15.0 bohr), and the  $\Gamma$ point approximation for Brillouin zone integration was adopted. The molecular geometry of trans-polyacetylene (bond lengths, bond angles, and lattice constant) was taken to be that of experiment. 46 The geometries for the substituted cases were generated by optimizing the atom positions of the substituent groups while fixing all other atoms. All atoms were represented by Hamann-Schluter-Chiang-Vanderbilt (HSCV) norm-conserving pseudopotentials, 47,48 and the PBE<sup>49</sup> generalized gradient approximation exchange-correlation approximation was used with a 40 Ry plane-wave cutoff energy for the Kohn-Sham (KS) orbitals. For integrating the time-dependent KS equation, we employed the maximum localized Wannier function (TD-MLWF) gauge.<sup>37</sup> enforced time-reversal symmetry (ETRS) integrator<sup>50</sup> was used with a 0.1 au integration step size. An electric field

 $\mathbf{E}(t) = \mathbf{A} \sin\left(\frac{2\pi}{T}t\right)$  was applied as the driving field, and we considered the time period T range of 50-300 au and the field amplitude |A| range of  $(2.0-7.0)\times 10^{-3}$  a.u. with uniform sampling intervals of 25 au and  $0.5\times 10^{-3}$  a.u., respectively. A time-dependent electric field was applied in the length gauge using the scalar potential in the KS Hamiltonian.<sup>37</sup>

#### ASSOCIATED CONTENT

# **Solution** Supporting Information

The Supporting Information is available free of charge at https://pubs.acs.org/doi/10.1021/acs.jpclett.3c01746.

Brief discussions of the Floquet topological pump in the unsubstituted *trans*-polyacetylene case and Floquet theory in TDDFT; overlap matrix, integrated current, and time-dependent particle population for dominant DTOs for differently substituted *trans*-polyacetylenes (PDF)

#### AUTHOR INFORMATION

# **Corresponding Author**

Yosuke Kanai — Department of Chemistry and Department of Physics and Astronomy, University of North Carolina at Chapel Hill, Chapel Hill, North Carolina 27514, United States; orcid.org/0000-0002-2320-4394; Email: ykanai@unc.edu

#### **Author**

Ruiyi Zhou — Department of Chemistry, University of North Carolina at Chapel Hill, Chapel Hill, North Carolina 27514, United States; orcid.org/0000-0002-7732-6338

Complete contact information is available at: https://pubs.acs.org/10.1021/acs.jpclett.3c01746

# Notes

The authors declare no competing financial interest.

# ACKNOWLEDGMENTS

This work was supported by the National Science Foundation under Awards CHE-1954894 and OAC-17402204. We thank Research Computing at the University of North Carolina at Chapel Hill for providing computational resources.

# REFERENCES

- (1) Thouless, D. J. Quantization of Particle Transport. Phys. Rev. B 1983, 27, 6083-6087.
- (2) Ma, W.; Zhou, L.; Zhang, Q.; Li, M.; Cheng, C.; Geng, J.; Rong, X.; Shi, F.; Gong, J.; Du, J. Experimental Observation of a Generalized Thouless Pump with a Single Spin. *Phys. Rev. Lett.* **2018**, *120*, No. 120501.
- (3) Cerjan, A.; Wang, M.; Huang, S.; Chen, K. P.; Rechtsman, M. C. Thouless Pumping in Disordered Photonic Systems. *Light: Sci. Appl.* 2020, 9, 178.
- (4) Guo, A.-M.; Hu, P.-J.; Gao, X.-H.; Fang, T.-F.; Sun, Q.-F. Topological Phase Transitions of Thouless Charge Pumping Realized in Helical Organic Molecules with Long-Range Hopping. *Phys. Rev. B* **2020**, *102*, No. 155402.
- (5) Zhang, Y.; Gao, Y.; Xiao, D. Topological Charge Pumping in Twisted Bilayer Graphene. *Phys. Rev. B* **2020**, *101*, No. 041410.
- (6) Nakajima, S.; Tomita, T.; Taie, S.; Ichinose, T.; Ozawa, H.; Wang, L.; Troyer, M.; Takahashi, Y. Topological Thouless Pumping of Ultracold fermions. *Nat. Phys.* **2016**, *12*, 296.

- (7) Lohse, M.; Schweizer, C.; Zilberberg, O.; Aidelsburger, M.; Bloch, I. A Thouless Quantum Pump with Ultracold Bosonic Atoms in an Optical Superlattice. *Nat. Phys.* **2016**, *12*, 350–354.
- (8) Hayward, A.; Schweizer, C.; Lohse, M.; Aidelsburger, M.; Heidrich-Meisner, F. Topological Charge Pumping in the Interacting Bosonic Rice-Mele Model. *Phys. Rev. B* **2018**, 98, No. 245148.
- (9) Friedman, A. J.; Gopalakrishnan, S.; Vasseur, R. Integrable Many-Body Quantum Floquet-Thouless Pumps. *Phys. Rev. Lett.* **2019**, 123, No. 170603.
- (10) Taherinejad, M.; Garrity, K. F.; Vanderbilt, D. Wannier Center Sheets in Topological Insulators. *Phys. Rev. B* **2014**, 89, No. 115102.
- (11) Li, R.; Fleischhauer, M. Finite-Size Corrections to Quantized Particle Transport in Topological Charge Pumps. *Phys. Rev. B* **2017**, 96, No. 085444.
- (12) Rice, M. J.; Mele, E. J. Elementary Excitations of a Linearly Conjugated Diatomic Polymer. *Phys. Rev. Lett.* **1982**, *49*, 1455–1459.
- (13) Privitera, L.; Russomanno, A.; Citro, R.; Santoro, G. E. Nonadiabatic Breaking of Topological Pumping. *Phys. Rev. Lett.* **2018**, 120, No. 106601.
- (14) Kuno, Y. Non-Adiabatic Extension of the Zak Phase and Charge Pumping in the Rice-Mele Model. *Eur. Phys. J. B* **2019**, 92, 195.
- (15) Fedorova, Z.; Qiu, H.; Linden, S.; Kroha, J. Topological Transport Quantization by Dissipation in Fast Thouless Pumps. In 2020 Conference on Lasers and Electro-Optics (CLEO): QELS\_Fundamental Science; Optical Society of America, 2020; Paper FM2A.3.
- (16) Oka, T.; Kitamura, S. Floquet Engineering of Quantum Materials. *Annu. Rev. Condens. Matter Phys.* **2019**, *10*, 387–408.
- (17) Rudner, M. S.; Lindner, N. H. Band Structure Engineering and Non-Equilibrium Dynamics in Floquet Topological Insulators. *Nat. Rev. Phys.* **2020**, *2*, 229–244.
- (18) Zhou, R.; Yost, D. C.; Kanai, Y. First-Principles Demonstration of Nonadiabatic Thouless Pumping of Electrons in a Molecular System. *J. Phys. Chem. Lett.* **2021**, *12*, 4496–4503.
- (19) Khoury, J. F.; Schoop, L. M. Chemical Bonds in Topological Materials. *Trends Chem.* **2021**, *3*, 700–715.
- (20) Martín Pendás, A.; Contreras-García, J.; Pinilla, F.; Mella, J. D.; Cardenas, C.; Muñoz, F. A Chemical Theory of Topological Insulators. *Chem. Commun.* **2019**, *55*, 12281–12287.
- (21) Castro, A.; De Giovannini; Sato, U.; Hübener, S. A.; Rubio, H. Floquet Engineering with Quantum Optimal Control Theory. *New J. Phys.* **2023**, 25, 043023.
- (22) Topp, G. E.; Jotzu, G.; McIver, J. W.; Xian, L.; Rubio, A.; Sentef, M. A. Topological Floquet Engineering of Twisted Bilayer Graphene. *Phys. Rev. Res.* **2019**, *1*, No. 023031.
- (23) Resta, R. Macroscopic Polarization in Crystalline Dielectrics: The Geometric Phase Approach. *Reviews of modern physics* **1994**, *66*, 899.
- (24) Nakagawa, M.; Slager, R.-J.; Higashikawa, S.; Oka, T. Wannier Representation of Floquet Topological States. *Phys. Rev. B* **2020**, *101*, No. 075108.
- (25) Aharonov, Y.; Anandan, J. Phase Change During a Cyclic Quantum Evolution. *Phys. Rev. Lett.* **1987**, *58*, 1593–1596.
- (26) Xiao, D.; Chang, M.-C.; Niu, Q. Berry Phase Effects on Electronic Properties. *Rev. Mod. Phys.* **2010**, *82*, 1959–2007.
- (27) Resta, R. Quantum-Mechanical Position Operator in Extended Systems. *Phys. Rev. Lett.* **1998**, *80*, 1800.
- (28) Vanderbilt, D. Berry Phases in Electronic Structure Theory: Electric Polarization, Orbital Magnetization and Topological Insulators; Cambridge University Press: Cambridge, U.K., 2018.
- (29) Yao, Y.; Yost, D. C.; Kanai, Y. K-Shell Core-Electron Excitations in Electronic Stopping of Protons in Water from First Principles. *Phys. Rev. Lett.* **2019**, *123*, No. 066401.
- (30) Yost, D. C.; Yao, Y.; Kanai, Y. First-Principles Modeling of Electronic Stopping in Complex Matter under Ion Irradiation. *J. Phys. Chem. Lett.* **2020**, *11*, 229–237.
- (31) Shepard, C.; Zhou, R.; Yost, D. C.; Yao, Y.; Kanai, Y. Simulating Electronic Excitation and Dynamics with Real-Time

- Propagation Approach to TDDFT within Plane-Wave Pseudopotential Formulation. J. Chem. Phys. 2021, 155, No. 100901.
- (32) Li, X.; Tully, J. C. Ab Initio Time-Resolved Density Functional Theory for Lifetimes of Excited Adsorbate States at Metal Surfaces. *Chem. Phys. Lett* **2007**, 439, 199–203.
- (33) Goings, J. J.; Lestrange, P. J.; Li, X. Real-Time Time-Dependent Electronic Structure Theory. *Wiley Interdiscip. Rev.: Comput. Mol. Sci.* **2018**, *8*, No. e1341.
- (34) Li, X.; Govind, N.; Isborn, C.; DePrince, A. E., III; Lopata, K. Real-Time Time-Dependent Electronic Structure Theory. *Chem. Rev.* **2020**, *120*, 9951–9993.
- (35) Tateyama, Y.; Oyama, N.; Ohno, T.; Miyamoto, Y. Real-Time Propagation Time-Dependent Density Functional Theory Study on the Ring-Opening Transformation of the Photoexcited Crystalline Benzene. *J. Chem. Phys.* **2006**, *124*, No. 124507.
- (36) Casida, M. E. Time-Dependent Density Functional Response Theory for Molecules. In *Recent Advances in Density Functional Methods, Part I;* World Scientific, 1995; pp 155–192.
- (37) Yost, D. C.; Yao, Y.; Kanai, Y. Propagation of Maximally Localized Wannier Functions in Real-Time TDDFT. *J. Chem. Phys.* **2019**, *150*, No. 194113.
- (38) Zhou, R.; Kanai, Y. Dynamical Transition Orbitals: A Particle—Hole Description in Real-Time TDDFT Dynamics. *J. Chem. Phys.* **2021**, *154*, No. 054107.
- (39) Runge, E.; Gross, E. K. U. Density-Functional Theory for Time-Dependent Systems. *Phys. Rev. Lett.* **1984**, *52*, 997–1000.
- (40) Yabana, K.; Bertsch, G. F. Time-Dependent Local-Density Approximation in Real Time. *Phys. Rev. B* **1996**, *54*, 4484–4487.
- (41) Schleife, A.; Draeger, E. W.; Anisimov, V. M.; Correa, A. A.; Kanai, Y. Quantum Dynamics Simulation of Electrons in Materials on High-Performance Computers. *Comput. Sci. Eng.* **2014**, *16*, 54–60.
- (42) Draeger, E.; Gygi, F. Qbox Code, Qb@ll Version; Lawrence Livermore National Laboratory, 2017.
- (43) Kononov, A.; Lee, C.-W.; dos Santos, T. P.; Robinson, B.; Yao, Y.; Yao, Y.; Andrade, X.; Baczewski, A. D.; Constantinescu, E.; Correa, A. A.; et al. Electron Dynamics in Extended Systems within Real-Time Time-Dependent Density-Functional Theory. *MRS Commun.* **2022**, *12*, 1002–1014.
- (44) Gygi, F. Architecture of Qbox: A Scalable First-Principles Molecular Dynamics Code. *IBM J. Res. Dev.* **2008**, *52*, 137–144.
- (45) Schleife, A.; Draeger, E. W.; Kanai, Y.; Correa, A. A. Plane-Wave Pseudopotential Implementation of Explicit Integrators for Time-Dependent Kohn-Sham Equations in Large-Scale Simulations. *J. Chem. Phys.* **2012**, *137*, No. 22A546.
- (46) Yannoni, C.; Clarke, T. Molecular Geometry of Cis-and Trans-Polyacetylene by Nutation Nmr Spectroscopy. *Physical review letters* **1983**, *51*, 1191.
- (47) Hamann, D. R.; Schlüter, M.; Chiang, C. Norm-Conserving Pseudopotentials. *Phys. Rev. Lett.* **1979**, 43, 1494–1497.
- (48) Vanderbilt, D. Optimally Smooth Norm-Conserving Pseudopotentials. *Phys. Rev. B* **1985**, 32, 8412–8415.
- (49) Perdew, J. P.; Burke, K.; Ernzerhof, M. Generalized Gradient Approximation Made Simple. *Phys. Rev. Lett.* **1996**, *77*, 3865–3868.
- (50) Castro, A.; Marques, M. A.; Rubio, A. Propagators for the Time-Dependent Kohn-Sham Equations. *J. Chem. Phys.* **2004**, *121*, 3425–3433.